Phase diagram of an Ising model for ultrathin magnetic films: Comparing mean field and Monte Carlo predictions

Santiago A. Pighín* and Sergio A. Cannas†
Facultad de Matemática, Astronomía y Física, Universidad Nacional de Córdoba, Ciudad Universitaria, 5000 Córdoba, Argentina
(Received 9 November 2006; revised manuscript received 3 March 2007; published 29 June 2007)

We study the critical properties of a two-dimensional Ising model with competing ferromagnetic exchange and dipolar interactions, which models an ultrathin magnetic film with high out-of-plane anisotropy in the monolayer limit. In this work, we present a detailed calculation of the (δ,T) phase diagram, δ being the ratio between exchange and dipolar interaction intensities. We compare the results of both mean field approximation and Monte Carlo numerical simulations in the region of low values of δ, identifying the presence of a recently detected phase with nematic order in different parts of the phase diagram, besides the well-known striped and tetragonal liquid phases. We also found that, in the regions of the phase diagram where Monte Carlo simulations display nematic order, the mean field approximation predicts hybrid solutions composed by stripes of different widths. Another remarkable qualitative difference between both calculations is the absence, in this region of the Monte Carlo phase diagram, of the temperature dependency of the equilibrium stripe width predicted by the mean field approximation.

DOI: 10.1103/PhysRevB.75.224433 PACS number(s): 75.70.Kw, 75.40.Mg, 75.40.Cx

I. INTRODUCTION

Many ultrathin magnetic films, e.g., Co/Cu, Co/Au, and Fe/Cu, undergo a reorientation transition at a temperature T_R; for temperatures below T_R, the spins align preferentially in a direction perpendicular to the film, while above T_R, they align in a magnetized state parallel to the plane of the film.[1–3] This reorientation transition is due to the competition between the in-plane part of the dipolar interaction and the surface anisotropy.[4] Furthermore, in the range of temperatures where the magnetization points out of the plane, the competition between exchange and dipolar interactions causes the global magnetization to be effectively zero but instead striped magnetic domain patterns emerge.[2,3,5] In the limit of a monolayer film, the following dimensionless Ising Hamiltonian emerges as a minimal model to describe many of the relevant physical properties of those materials:[3]

$$\mathcal{H} = -\delta \sum_{\langle i,j \rangle} S_i S_j + \sum_{(i,j)} \frac{S_i S_j}{r_{ij}^3}, \tag{1}$$

where δ stands for the ratio between the exchange $J_0>0$ and the dipolar $J_d>0$ interaction parameters, i.e., $\delta=J_0/J_d$. The first sum runs over all pairs of nearest-neighbor Ising spins $S_i=\pm 1$ in a square lattice and the second one over all distinct pairs of spins of the lattice (every pair is counted once); r_{ij} is the distance, measured in crystal units, between sites i and j and the energy is measured in units of J_d. In spite of intense theoretical work,[3,6–15] there are still many important open questions regarding the critical properties of this model. A detailed understanding of those critical properties is the cornerstone of the theoretical framework needed to explain complex phenomena in ultrathin magnetic films, such as the recently observed inverse transition in Fe on Cu films.[5]

The main difficulties to analyze the critical properties of this model are related to the long-range character of the dipolar interactions, which, combined with the frustration derived from the competition between interactions, adds to any theoretical approach an extra degree of complexity. Then, even the simplest approach, namely, mean field (MF) approximation, leads to an infinite number of coupled equations that, except for some particular situations, cannot be solved exactly. For instance, in an early work, Czech and Villain[6] derived an exact expression for the MF critical temperature between the disordered and the modulated (striped) phases; however, for subcritical temperatures, the determination of any property must rely on numerical solutions of the mean field equations or further ansatz has to be introduced[16] to obtain *approximated* solutions of the MF equations. An example is the temperature dependency of the equilibrium stripe width; being experimentally accessible,[16] reliable theoretical predictions of this property could be very important to understand the basic mechanisms behind the complex behavior observed in these materials. Though MF is a powerful theoretical tool, it is known that, even when the corresponding equations can be solved exactly, neglecting fluctuations can introduce qualitative changes in the critical behavior. Therefore, it is important to compare MF predictions with those obtained by other methods, in order to establish the limits of validity of the approximation.

A natural way to check the mean field predictions is to contrast them with Monte Carlo (MC) simulations. However, the long-range order nature of the dipolar interactions makes it very difficult to simulate large system sizes. The ground-state stripe width h is the natural length scale in these problems. Hence, in order to avoid strong finite-size effects, the simulations must be carried out for system sizes $L \gg h$; this restricts the simulations to situations in which h is much smaller than the experimentally observed values (typical values of the stripe width in Fe on Cu films, for instance, are of the order[16,17] of 1 μm, which corresponds roughly to $h=4000$ lattice constants). Since the ground-state value of h increases exponentially with[18] δ, the values of δ available for simulations are about of 1 order of magnitude smaller than the realistic values.

In this work, we carried out a detailed analysis of the equilibrium phase diagram of this model in the (δ,T) space

for low values of δ, i.e., for $0 \leqslant \delta \leqslant 4$, which corresponds to stripe widths $h \leqslant 7$. By extending the Czech and Villain[6] MF approach to the low-temperature region of the phase diagram, we performed in Sec. II a detailed analysis of the different transition lines between striped states, by solving numerically the MF equations. Those results are compared in Sec. III with MC simulations that refine previous results[7,10,11,13–15] and extend them to other regions of the phase diagram. Our results show that, at least in the analyzed region of the phase diagram, several discrepancies are observed between both phase diagrams, which are discussed in Sec. IV.

II. MEAN FIELD PHASE DIAGRAM

The Hamiltonian (1) can be rewritten as

$$\mathcal{H} = -\frac{1}{2}\sum_{i,j} J_{ij} S_i S_j, \tag{2}$$

where

$$J_{ij} = \begin{cases} \delta - 1 & \text{if } i,j \text{ are nearest neighbors} \\ 0 & \text{if } i = j \\ -\dfrac{1}{r_{ij}^3} & \text{otherwise.} \end{cases} \tag{3}$$

A straightforward way to derive a mean field theory for this Hamiltonian is the usage of the variational MF free energy per particle:[19]

$$f_{\mathrm{MF}} = \frac{1}{N}\langle \mathcal{H} \rangle_\rho + \frac{1}{\beta N}\langle \ln \rho \rangle_\rho, \tag{4}$$

where $N = L \times L$ is the system size, we have taken $k_B = 1$ and the averages are taken using the independent particle density matrix $\rho = \Pi_i \rho_i$; the one particle density matrices are subjected to the constraints:

$$\sum_{S_i = \pm 1} \rho_i = 1, \quad \sum_{S_i = \pm 1} S_i \rho_i = m_i.$$

Using the local order parameters m_i as variational parameters, we obtain the free-energy functional

$$f_{\mathrm{MF}}[\{m_i\}] = -\frac{1}{2N}\sum_{i,j} J_{ij} m_i m_j + \frac{1}{2\beta N}\sum_i [(1+m_i)\ln(1+m_i) + (1-m_i)\ln(1-m_i)]. \tag{5}$$

Minimizing Eq. (5) with respect to the order parameters m_i leads to the set of MF equations

$$m_i = \tanh\left(\beta \sum_{j=1}^{N} J_{ij} m_j\right), \quad i = 1, \ldots, N. \tag{6}$$

Assuming periodic boundary conditions, we introduce the Fourier transforms

$$m_i = \frac{1}{\sqrt{N}}\sum_{\vec{k}} \hat{m}_{\vec{k}} e^{i\vec{k}\cdot\vec{r}_i}, \tag{7}$$

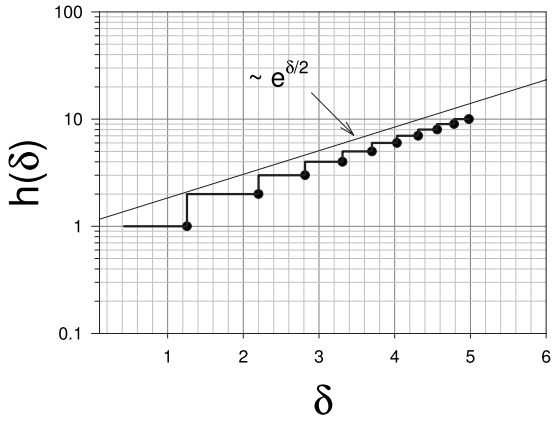

FIG. 1. Equilibrium stripe width as a function of δ at $T=0$. Filled circles indicate the values of delta at which two adjacent striped configurations take the same energy.

$$\hat{J}(\vec{k}) = \sum_i J_{0i} e^{-i\vec{k}\cdot(\vec{r}_i - \vec{r}_0)} = 2\delta(\cos k_x + \cos k_y) - \sum_i \frac{1}{r_{ij}^3}\cos(\vec{k}\cdot\vec{r}_{ij}), \tag{8}$$

where $\vec{r}_i$ is the position vector of site i, $\vec{r}_{ij} \equiv \vec{r}_i - \vec{r}_j$, $\hat{m}_{-\vec{k}} = \hat{m}_{\vec{k}}^*$ and the wave vectors $\vec{k}$ are restricted to the first Brillouin zone. Expanding the logarithms, Eq. (5) can be rewritten as

$$f_{\mathrm{MF}} = \frac{1}{2N}\sum_{\vec{k}} [T - \hat{J}(\vec{k})]|\hat{m}_{\vec{k}}|^2 + \frac{1}{\beta N}\sum_i \sum_{j=2}^{\infty}\left(\frac{1}{2j-1} - \frac{1}{2j}\right) m_i^{2j}, \tag{9}$$

which has the form of a Landau expansion. From this expression, it is immediate that a second-order transition between the disordered phase, $\hat{m}_{\vec{k}} \equiv 0 \, \forall \vec{k}$, and an ordered phase, with nonzero-order parameters, happens at the critical temperature:[6]

$$T_c = \max_{\vec{k}} \hat{J}(\vec{k}). \tag{10}$$

We calculated $T_c(\delta)$ by solving Eq. (10) numerically.

Equation (6) can now be written as

$$m_i = \tanh\left[\frac{\beta}{\sqrt{N}}\sum_{\vec{k}} \hat{m}_{\vec{k}} e^{i\vec{k}\cdot\vec{r}_i}\hat{J}(\vec{k})\right], \quad i = 1, \ldots, N. \tag{11}$$

We analyzed numerically the solutions of Eq. (11) for temperatures $T < T_c$ and $0 < \delta \leqslant 4$. In particular, we analyzed the solutions that share the symmetries of the different ground states, namely, antiferromagnetic (AF) and striped solutions. For $\delta < 0.425$, the ground state is antiferromagnetic,[7] while for $\delta > 0.425$, the ground state is composed by stripes of width $h(\delta)$. For large values of δ, we have[7] $h(\delta) \sim e^{\delta/2}$; for small values of δ, the equilibrium values of h can be easily evaluated numerically by comparing the energies of different striped configurations of increasing finite system sizes (they converge very quickly). $h(\delta)$ is shown in Fig. 1, where we

see that it attains the asymptotic exponential behavior for rather small values of δ.

At low but finite temperatures, the local magnetization inside the stripes decreases, i.e., $|m_i|<1$. Let us consider, for instance, a vertical striped state of width h. We demand the solutions of Eq. (11) to satisfy the conditions $m_{(x+h,y)}=-m_{(x,y)}\,\forall x,y$ and $m_{(x,y)}=m_{(x,y')}\,\forall x,y,y'$. This restricts the harmonics in Eq. (7) to those satisfying $(k_x,k_y)=[\pm(2l+1)\pi/h,0]$, with l an integer such that $2l+1\leq h$. For instance, for $h=1$, we only have $k_x=\pi$; for $h=2$, we have $k_x=\pm\pi/2$; for $h=3$, we have $k_x=\pm\pi/3,\pi$; etc. In other words, for a stripe solution of width h, we have h independent complex amplitudes $\hat{m}_{\vec{k}}$. In order to obtain pure real solutions, we must impose $\hat{m}^*_{\vec{k}}=\hat{m}_{-\vec{k}}$. Replacing those conditions into Eqs. (7) and (11) leads to a set of h nonlinear algebraic equations for the amplitudes that can be solved numerically. To solve those equations, we must evaluate $\hat{J}(k_x,0)$ from Eq. (8). A suitable approximation for that function is (see Appendix)

$$\hat{J}(k_x,0)\approx 2\delta(\cos k_x+1)-k_x^2+2\pi|k_x|-\frac{2\pi^2}{3}-2\zeta(3), \tag{12}$$

where $\zeta(x)$ is the Riemann zeta function. For the antiferromagnetic solution $m_{(x,y)}=m_0(-1)^{x+y}$, we have to compute

$$\hat{J}(\pi,\pi)=-4\delta+3\zeta(3)-4\sum_{x=1}^{\infty}(-1)^x\sum_{y=1}^{\infty}\frac{(-1)^y}{(x^2+y^2)^{3/2}}, \tag{13}$$

where the last term is calculated numerically. We calculated the MF stripe solutions for $h=1,\ldots,6$ for a wide range of values of $(\delta,T<T_c)$. To discriminate whether they are actually minima, we analyzed the second derivatives of the free energy. For every value of h, we first analyzed the stability of the solutions, that is, for every value of δ, we calculated the temperature $T_s(\delta)$ above which nontrivial solutions of the above described type cease to exist. This can be done by linearizing the corresponding set of equations around $\hat{m}_{\vec{k}}=0$ and demanding the condition of nontrivial solution, i.e., zero determinant of the linearized equations; this leads to the expression

$$T_s(\delta,h)=\hat{J}\left(\frac{\pi}{h},0\right). \tag{14}$$

The stability lines are shown in Fig. 2, together with $T_c(\delta)$. It can be seen that for large values of δ, the stability lines accumulate near the order-disorder transition line $T_c(\delta)$, implying an increasingly large number of metastable states as δ increases. Another remarkable fact is the presence of regions near $T_c(\delta)$ where no striped solutions exist (see Fig. 2). In those regions, another type of solutions appears, which are composed by parallel ferromagnetic stripes of different widths. We called them hybrid states. The hybrid states, which we denote by $<h_1^{n_1}h_2^{n_2}\cdots h_l^{n_l}>$, following the notation of Selke and Fisher[20] for the axial next-nearest-neighbor Ising model (ANNNI), consists in the periodic repetition of a

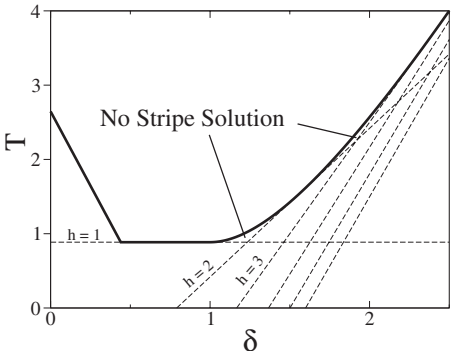

FIG. 2. Stability lines $T_s(\delta,h)$ for the MF striped solutions at finite temperatures (dashed). Full line: critical temperature $T_c(\delta)$.

fundamental pattern composed by n_1 stripes of width h_1 (with opposite orientation), followed by n_2 stripes of width h_2, and so on. The regions where the hybrid states appear are shown in the MF phase diagram presented in Fig. 3. The boundaries between ordered phases (corresponding to first-order transitions) were determined by comparing the free energies of the different solutions (striped and hybrid) using Eq. (5); they are shown by dashed lines in Fig. 3. We found that the hybrid states appear through a sort of branching process near the boundary between two stable striped solutions as the temperature approaches T_c from below. For instance, the transition line between the striped phases $h=1$ and $h=2$ ends in a triple point where a stable phase $\langle 1\,2\rangle$ appears between them; as we increase δ, the transition line between the striped phase $h=2$ and the hybrid one $\langle 1\,2\rangle$ bifurcates in a new triple point giving rise to the appearance of a $\langle 12^2\rangle$ phase between the $\langle 1\,2\rangle$ and the $h=2$ and so on (see inset of Fig. 3). As the temperature increases, more complicated hybrid states proliferate (we just show a few of them in Fig. 3

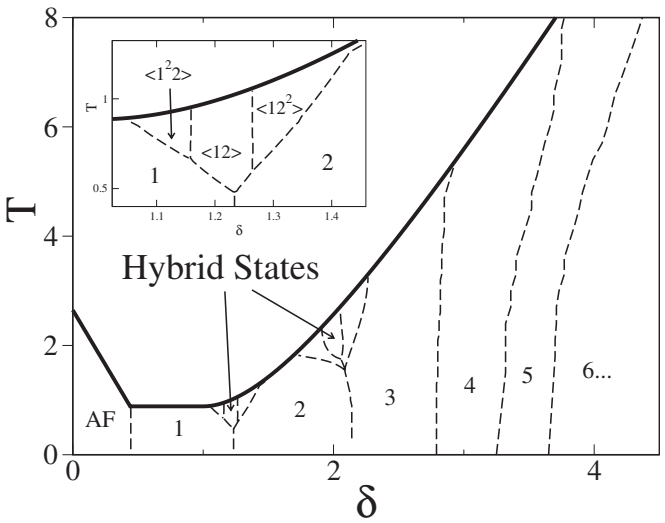

FIG. 3. Mean field phase diagram. The numbers in the low-temperature region indicate the equilibrium stripe width h of the phases. Dashed lines correspond to first-order phase transition between ordered phases; the full line corresponds to the critical temperature $T_c(\delta)$. Inset: Zoom of the hybrid region near the boundary between the striped phases $h=1$ and $h=2$.

as an example), in a completely analogous way as in a related model, namely, the three-dimensional Ising model with competing short-range ferromagnetic interactions and long-range Coulomb interactions.[21] The MF phase diagram of that model is very similar to that of the present one, the striped states being replaced by lamellar ones.

Finally, we found evidences that the proliferation of hybrid states also happens near the boundary between striped phases with larger widths (for instance, 3 and 4), but they appear very close to T_c and the computational effort needed to obtain an accurate estimation of the phase boundaries becomes very high.

III. MONTE CARLO PHASE DIAGRAM

Different parts of the phase diagram of this model were analyzed by different authors using MC numerical simulations, for small values of δ and small system sizes.[7,8,10,12,14,15] In this section, we extend those results to other parts of the phase diagram and to larger system sizes (in some cases), in order to obtain a complete description of the small-δ phase diagram that can be compared with the MF phase diagram.

The MC results were obtained using heat bath dynamics on $N=L\times L$ square lattices with periodic boundary conditions (Ewald sums were used to handle it[3]). We analyzed the equilibrium behavior of different quantities for system sizes running from $L=24$ to $L=84$; the maximum sizes used for each quantity were chosen according to the associated computational effort.

The first quantity we calculated was the order-disorder transition temperature as a function of δ, which we called $T_c^{(2)}(\delta)$ [analogous to $T_c(\delta)$ in the MF case]. This quantity was determined by means of the specific heat

$$C(T) = \frac{1}{NT^2}(\langle H^2\rangle - \langle H\rangle^2), \tag{15}$$

where $\langle\cdots\rangle$ stands for a thermal average. For some values of δ, we also calculated the fourth-order cumulant

$$V(T) = 1 - \frac{\langle H^4\rangle}{3\langle H^2\rangle^2} \tag{16}$$

to characterize the order of the phase transition.

At intermediate high temperatures (close to the order-disorder transition and above it), this system presents a partially disordered phase with broken orientational order called *tetragonal liquid*.[3,8,12–14] It is characterized by domains of stripes with mutually perpendicular orientations forming a kind of labyrinthine structure. At higher temperatures, these domains collapse and the system crosses over continuously to a completely disordered phase (paramagnetic), without a sharp phase transition between them.[3] While the existence of the tetragonal liquid phase has been clearly established by MC simulations, it is completely absent in the MF approximation (we discuss this point in Sec. IV). MC simulations also showed recently[14] that for $\delta=2$, an intermediate phase with nematic order is present between the tetragonal liquid and the striped phase. The nematic phase is characterized by

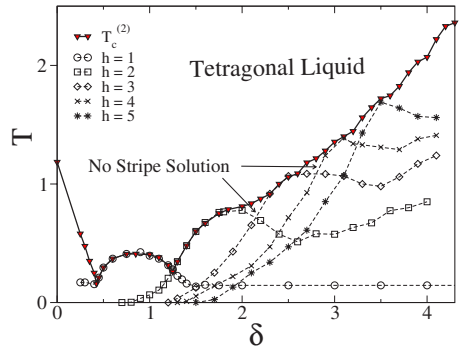

FIG. 4. (Color online) Order-disorder transition temperature $T_c^{(2)}(\delta)$ and striped stability lines $T_s(\delta)$ for different values of h (see text for details).

positional disorder and long-range orientational order and is consistent with one of the two possible scenarios predicted by a continuum approximation for ultrathin magnetic films in Refs. 22 and 23. The presence of the nematic phase is reflected (among several manifestations) in the appearance of two distinct maxima at different temperatures in the specific heat, associated with the stripe-nematic and the nematic-tetragonal liquid phase transitions, respectively. On the other hand, it was shown that for $\delta=1$, the specific heat presents a unique maximum, consistent with a direct transition from the tetragonal liquid to the striped phase,[14] suggesting that the nematic phase is only present for some range of values of δ. We will call $T_c^{(2)}$ the temperature of the high-temperature peak of the specific heat, whenever it presents two peaks, or the temperature of the unique peak if only one is present (for the system sizes considered and between the precision of the calculation). We will call $T_c^{(1)}$ the temperature of the low-temperature peak of the specific heat when it presents two peaks. While the calculation of $T_c^{(2)}$ is relatively easy, the calculation of $T_c^{(1)}$ is much more complicated and subtle, as it will be discussed below. $T_c^{(2)}$ was calculated for different values of $0\leqslant\delta\leqslant 4.2$ using the following simulation protocol: for each value of δ, we let first the system thermalize at a high enough temperature (such that it is in the disordered phase) during 10^5 Monte Carlo steps (MCS); after that, we calculated the specific heat for decreasing temperatures, down to a temperature well below the transition region. For every temperature, we took the final configuration of the previous one and discarded the first 2×10^4 MCS for thermalization and averaged over 10^5 MCS. Every curve was averaged then over 40 independent runs. This calculation was performed for system sizes $L\sim 50$ for all the values of δ, in order to make the finite-size bias comparable (for every value of δ, we choose the closer value of L commensurated with the modulation $2h$ of the corresponding ground-state width). The results are shown by triangles joined by a continuous line in Fig. 4. The order of the associated phase transition will be discussed in Sec. IV.

We next calculated the stability of the striped phases in different parts of the phase diagram. It was shown in Ref. 10 that the striped phases can remain in a metastable state for values of δ such that the equilibrium ground-state width corresponds to a different stripe width. Following the same pro-

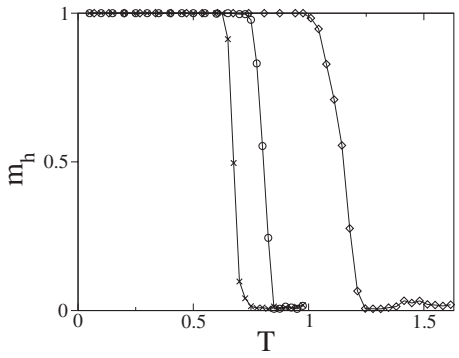

FIG. 5. Staggered magnetization for different δ and h values: $h=2$, $\delta=3.4$, and $L=60$ (×); $h=3$, $\delta=4.1$, and $L=48$ (◇); and $h=5$, $\delta=2.9$, and $L=40$ (○).

cedure as in Ref. 10, we analyzed the striped staggered magnetization

$$m_h = \frac{1}{N}\left\langle \left| \sum_{x,y} (-1)^{f_h(x)} S_{x,y} \right| \right\rangle, \tag{17}$$

where[3] $f_h(x)=[i-\mathrm{mod}(x,h)]/h$ and $x,y=1,\ldots,N$. This quantity takes the value of 1 in a completely ordered vertical striped state of width h and zero in a disordered state (paramagnetic, tetragonal, or nematic). Starting from an initially ordered vertical striped state at zero temperature, we increase the temperature up to high temperatures, averaging m_h at every step and using a similar procedure as for the calculation on $T_c^{(2)}$, but averaging over 10^6 MCS for every temperature to diminish metastability effects (see discussion below). We repeated this calculation for different values of δ, for each value of h; for every value of δ, the curve $m_h(T)$ was averaged over 25 independent runs. Typical curves $m_h(T)$ are shown in Fig. 5 for different values of h and δ. From these curves, we estimated the stability lines $T_s(\delta)$ (i.e., the temperature above which $m_h=0$) for $h=1,\ldots,5$ and $0<\delta<4.1$. The stability lines are shown in Fig. 4.

As in the MF case, we observe the existence of regions below $T_c^{(2)}$ where no stable striped solutions exist, at least up to $\delta=3$; for values of $\delta>3$, the data become very noisy (probably due to finite-size effects) and the large error bars do not allow us to identify clearly those regions for the present system sizes. We found that the equilibrium phase in those regions is a nematic one, instead of a hybrid state, as in the MF case (we checked the possible presence of hybrid states in those regions and they always decay after a short time into a nematic one). The nematic phase is characterized by an algebraic decay of the spatial spin-spin correlations in one of the coordinate directions and an exponential decay in the other. This can be studied through the structure factor (Fourier transform of the correlation function)

$$\mathcal{S}(\vec{k}) \equiv \langle |\hat{S}_{\vec{k}}|^2 \rangle, \tag{18}$$

where $\hat{S}_{\vec{k}}=\frac{1}{N}\Sigma_i S_i e^{-i\vec{k}\vec{r}_i}$. Cannas *et al.*[14] calculated an approximate expression for the nematic phase structure factor

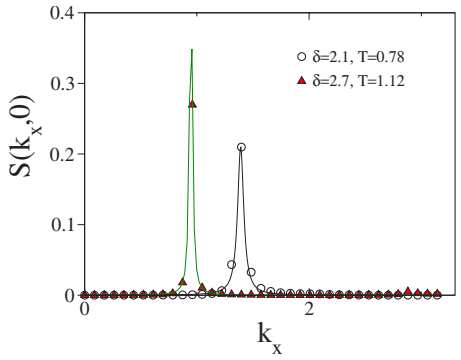

FIG. 6. (Color online) Structure factor for a $L=72$ system with $\delta=2.1$, $T=0.78$ (○) and $\delta=2.7$, $T=1.12$ (◇). Continuous lines correspond to fittings using Eq. (19): for $\delta=2.1$, $T=0.78$, we obtained $\lambda=0.033$, $k_0=1.39$; for $\delta=2.7$, $T=1.12$, $\lambda=0.0149$, $k_0=0.947$. $S(0,k_y)=0\,\forall\, k_y$ in both cases.

$$\mathcal{S}(\vec{k}) \approx \frac{\delta_{k_y,0}}{2\sqrt{N}}\left[\frac{\lambda}{(k_x-k_0)^2+\lambda^2}+\frac{\lambda}{(k_x+k_0)^2+\lambda^2}\right]. \tag{19}$$

We ran simulations for $L=72$ and different δ values in the uncovered regions. The system was slowly heated from zero temperature using the same process described above up to a temperature in the uncovered region, where we calculated $\mathcal{S}(\vec{k})$ by averaging over 2×10^5 MCS. The typical observed behavior of $\mathcal{S}(\vec{k})$ is shown in Fig. 6, together with Lorentzian fittings using Eq. (19); two typical spin configurations in corresponding regions can be seen in Fig. 7 (compare with the results of Ref. 14).

Following the same steps as in the MF case, we calculated next the transition lines between different phases at low temperature. The transition lines were obtained by comparing the free energies of the striped phases of widths h and $h+1$. The system size was chosen in these calculations to be a multiple of both $2h$ and $2(h+1)$. In what follows, we will assume that the free energy of a metastable state can be obtained by following a thermodynamical path (that is, a close sequence of equilibrated states) from a thermodynamically stable reference state. To calculate the free energy of a striped phase of width h, we first computed the internal energy per spin $u(T,\delta_i)\equiv\langle H\rangle/N$ along a quasistatic path from an initially low temperature T_0 up to a working temperature $T<T_s(\delta_i)$ keeping δ_i constant and taking the initial spin configuration of a given temperature as the final configuration of

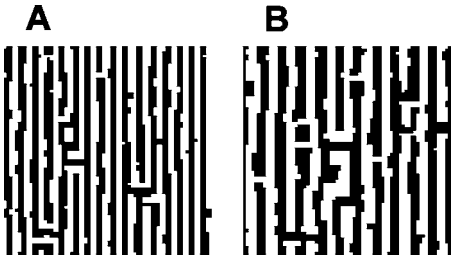

FIG. 7. Typical nematic spin configurations for $L=72$. (A) $\delta=2.10$, $T=0.78$; (B) $\delta=2.70$, $T=1.12$.

the previous one; the value of δ_i was chosen well separated from the border value at zero temperature between the striped phases of widths h and $h+1$. The free energy was then obtained by numerically integrating the thermodynamic relation

$$\beta f_h(\beta,\delta_i) = \beta_0 f_h(\beta_0,\delta_i) + \int_{\beta_0}^{\beta} u(\beta',\delta_i)d\beta', \qquad (20)$$

where $\beta=1/T$ and $\beta_0=1/T_0$. Once we arrive to the final configuration at (T,δ_i), we perform a second quasistatic path at constant temperature, by slowly changing δ, up to a final value δ_f corresponding to a striped ground state of width $h+1$. Along this path, we measure the average exchange energy

$$u_{ex}(\beta,\delta) \equiv -\frac{1}{N}\left\langle \sum_{\langle i,j\rangle} S_i S_j \right\rangle. \qquad (21)$$

From the expression,

$$f = -\frac{1}{N\beta}\log \mathcal{Z}, \qquad (22)$$

where $\mathcal{Z}$ is the partition function, is easy to see that

$$\frac{\partial f}{\partial \delta} = u_{ex}(\beta,\delta). \qquad (23)$$

Hence, the free energy along the last path can be obtained by numerically integrating the equation

$$f_h(\beta,\delta) = \int_{\delta_i}^{\delta} u_{ex}(\beta,\delta')d\delta' + f_h(\beta,\delta_i). \qquad (24)$$

Repeating the same procedure for the striped phase $h+1$, but following the second path in the inverse sense (i.e., decreasing δ from δ_f down to δ_i), we calculated the free energy $f_{h+1}(\beta,\delta)$ at the same temperature. The transition point $\delta_t(T)$ is obtained from the equation $f_h(\beta,\delta_t)=f_{h+1}(\beta,\delta_t)$. We calculated the first-order transition lines between striped phases up to $h=6$. The results are shown in the MC phase diagram of Fig. 8 (the transition lines between the AF and the $h=1$ and between the $h=1$ and $h=2$ phases were already calculated in Ref. 10; we put it here for completeness). Notice that all the calculated transition lines are almost independent of T, at variance with the MF prediction.

We next analyzed the transition temperature $T_c^{(1)}$ between the nematic and the striped phases. In order to check whether the stability lines $T_s(\delta)$ can be used to estimate $T_c^{(1)}$, we analyzed the behavior of the specific heat and fourth-order cumulant [Eqs. (15) and (16)] around the regions below $T_c^{(2)}$ where no striped states exist. The simulation protocol used to determine $T_c^{(2)}$ is completely unable to detect the low-temperature transition at $T_c^{(1)}$. This is because free-energy barriers associated with both transitions for the system sizes here considered are larger around $T_c^{(1)}$ than around $T_c^{(2)}$, as was shown in Ref. 14. Indeed, a rough estimation of the average times needed by the system to jump the free-energy barrier between the striped and the nematic phases is of the order of the millions of MCS, thus generating a strong metastability when the average times are of the order of 10^5 MCS.[24] In Ref. 14, it was shown that an accurate estimation of $T_c^{(1)}$ for $\delta=2$ requires, for every temperature, average times of the order of 2×10^8 MCS. However, we verified that an average time of 5×10^7 is enough to determine $T_c^{(1)}$ between the error bars we are using in the present calculation (although such time scales are not enough to determine the height of the specific-heat maximum with precision and therefore to allow a finite-size scaling analysis). In order to save computational effort, we used the following procedure for fixed values of δ around the regions of interest: first, we ran the same simulation protocol as for $T_c^{(2)}$ down to low temperatures and repeated it for the same parameter values, but heating from a low temperature up to high temperatures and taking as initial configuration the ordered striped state. In both cases, we calculated the internal energy $u(T)$ along the path. This allowed us to determine the approximated location of $T_c^{(1)}$, by looking at the temperature range where the internal energy exhibits metastability.[24] Then, we calculated C and V for a limited set of temperatures in that region, by taking averages for each temperature over a single MC run of 5×10^7 MCS. In order to get a more accurate estimation of $T_c^{(2)}$ for the same values of δ, we also repeated the latter calculation for temperatures around the previous estimation of $T_c^{(2)}$ taking averages over 10^7 MCS. These calculations were performed for $\delta=2.1$ and 2.25 (near the $h=1-h=2$ border) with $L=48$. The behavior of C and V for $\delta=2.25$ is shown in Fig. 9 (compare with the results of Ref. 14). We verified that the location of the low-temperature peak of C coincides between the error bars with the value of $T_s(\delta)$ for the same values of δ. The values of $T_c^{(1)}$ for $\delta=2$ (from Ref. 14), $\delta=2.1,2.25$ (from the above calculation), and $\delta=2.7,2.8,2.9$ (estimated from the stability lines) are shown by diamonds in the MC phase diagram of Fig. 8. Reliable calculations of $T_c^{(1)}$ for larger values of δ would require sys-

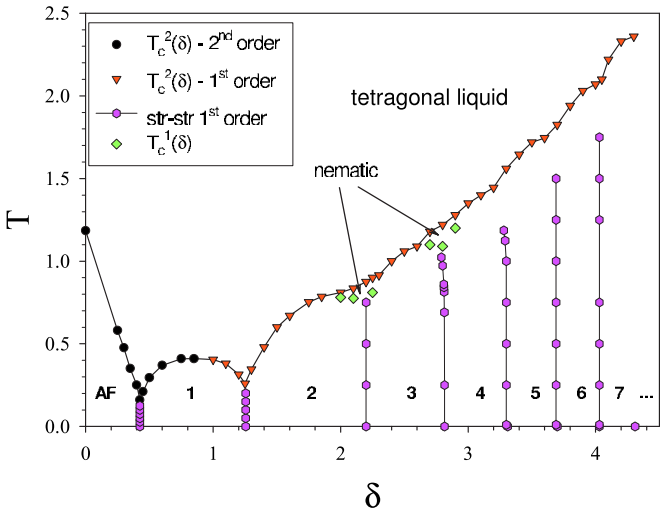

FIG. 8. (Color online) Monte Carlo phase diagram. The numbers indicate the equilibrium width of the low-temperature striped phases. The order of the different phase-transition lines is indicated in the inset (see text for details). The continuous lines are a guide to the eyes.

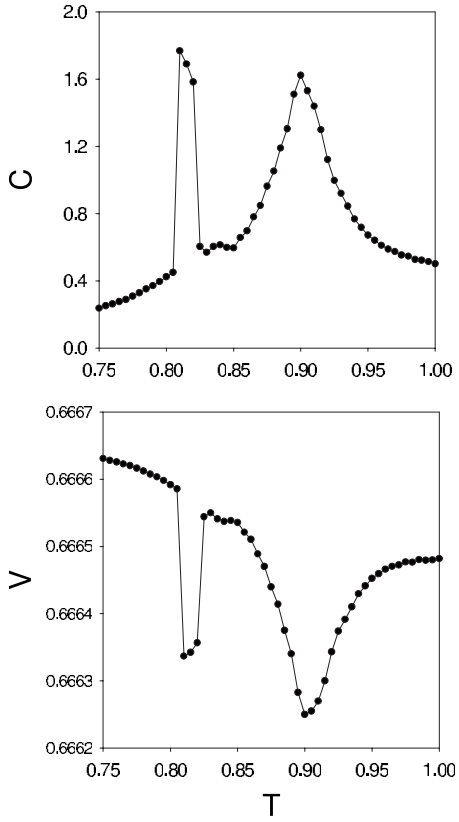

FIG. 9. Specific heat and fourth-order cumulant as a function of T for $\delta=2.25$ and $L=48$.

tem sizes that are out of the present computational capabilities.

IV. DISCUSSION

We have presented a detailed calculation of the finite temperature phase diagram of the Ising dipolar model in the range $0 \leqslant \delta \leqslant 4$, which allow striped ground-state configurations of width up to $h=7$. We compared the predictions of MF approximation with extensive MC numerical simulations. Although the overall appearance of both phase diagrams looks similar, several differences are remarkable.

The first difference to be noticed is the absence of nematic and tetragonal orders in the MF approximation. This results from the fact that both phases are spatially disordered, which implies that $\langle \hat{S}_{\vec{k}} \rangle = \hat{m}_{\vec{k}} = 0 \, \forall \, \vec{k}$. The characteristic features of those states, namely, the broken rotational symmetry of the nematic state and the discrete rotational symmetry of the tetragonal state, can only be observed when looking at the behavior of the spatial correlations or, equivalently, of the structure factor[3,14] [Eq. (19)]. Since fluctuations are neglected in the MF approximation, it follows that $\mathcal{S}(\vec{k}) = \hat{m}_{\vec{k}} \hat{m}_{-\vec{k}} = 0$ and therefore the only possible spatially disordered solution within this approximation is the paramagnetic one. On the other hand, the MF approximation presents hybrid state solutions in the regions of the phase diagram where MC predicts only nematic order. Moreover, we verified that hybrid states are unstable in that regions, suggesting that (in the language of renormalization group) fluctuations play the role of a relevant scaling field that turns the MF hybrid fixed points unstable toward nematic attractors (in some sense, the hybrid states could be the closest state to a nematic one that can be obtained when fluctuations are neglected). This would be consistent with the fact that fluctuations, when included, can modify the continuous nature MF prediction for the phase transition between the high-temperature disordered phase and the low-temperature ordered one: Hartree approximation applied to the continuous version of Hamiltonian (1) predicts a fluctuation-induced first-order transition of *any finite* value of δ,[12] which continuously fades out for increasing values of δ.[24] In fact, MC simulations show a more complex scenario, where the nature of the order-disorder phase transition at $T_c^{(2)}$ depends on the value of δ.

Rastelli *et al.* have shown that for $\delta=0$, the transition is indeed continuous and belongs to the universality class of the nearest-neighbor Ising model.[15] They also found a rather clear evidence of a second-order transition for $\delta=0.85$, but with an unusual value for the critical exponent β.[15] However, Cannas *et al.* have shown that for $\delta=1$, the system presents a weak first-order phase transition.[14] These results are consistent with the presence of a second-order transition line for small values of δ that joins with continuous slope a first-order transition line for larger values of δ at a tricritical point somewhere between $\delta=0.85$ and $\delta=1$ and the unusual critical exponents at $\delta=0.85$ are probably due to a crossover effect near the tricritical point. There are also clear evidences that the transition is first order for $\delta=2$ (Refs. 12 and 14) and $\delta=1.7, 2.5$ (Ref. 15). The behavior of the fourth-order cumulant observed in the present work for $\delta=2.1$ and $\delta=2.25$ is also consistent with a first-order transition. For $\delta=3$, the results of Rastelli *et al.*[15] appear to suggest that the transition becomes continuous again. However, this is a matter of debate,[24] and numerical results using a completely different technique[13] for $\delta=4.45$ are also consistent with a first-order transition.

We also presented numerical evidences of the presence of an intermediate nematic phase between the disordered and the striped ones in different parts of the phase diagram. Although it seems that the nematic phase is only located near the border lines between striped states, the presence of this phase in other regions in narrow ranges of temperatures cannot be excluded and larger system sizes should be required to clarify this.

The existence of both types of scenarios for relatively large values of δ, namely, one direct first-order transition from the striped phase to the tetragonal liquid or two phase transitions with an intermediate nematic phase, would be in qualitative agreement with theoretical predictions based on a continuous approach.[22,23] It is worth mentioning that Abanov *et al.*[23] conjectured a second-order nematic-tetragonal phase transition; since their whole analysis is based on mean field arguments, the disagreement with the MC results can be understood from the fluctuation-induced nature of the transition (see the discussion in Refs. 12 and 14). Regarding the order of the transition at $T_c^{(1)}(\delta)$, the situation is less clear. Cannas *et al.*[14] have shown for $\delta=2$ that, even when the finite-size scaling is consistent with a first-order transition, the energy changes continuously at $T_c^{(1)}(\delta)$ in the thermodynamic limit;

this produces a saturation in the associated specific-heat peak behavior that strongly resembles that observed in a Kosterlitz-Thouless (KT) transition. That could be indicative of the emergency of smectic order between the nematic and the striped phases for larger system sizes and would be in qualitative agreement with theoretical predictions based on a continuous approach.[22,23] If that would be the case, probably our calculation of $T_c^{(1)}(\delta)$ overestimates the true transition temperature, since it is known that the specific-heat peak locates above the KT transition temperature,[19] and therefore the nematic phase would extend in larger regions of the phase diagram. However, at the present level, it is very difficult to improve this estimation due to finite-size effects.

Regarding the low-temperature behavior, a remarkable prediction of both MF and MC is the existence of an increasingly large number of striped metastable states as δ increases.

Finally, we found that, at variance with the MF prediction, up to $\delta=4$, the transition lines between striped phases that are completely vertical imply temperature independence of the stripe width. This suggests the existence of some large threshold value of δ, above which wall fluctuations make the system to cross over to a "mean field regime," where it starts to exhibit temperature dependency of the stripe width.

ACKNOWLEDGMENTS

Fruitful discussions with D. A. Stariolo, F. A. Tamarit, P. M. Gleiser, D. Pescia, A. Vindigni, and O. Portmann are acknowledged. This work was partially supported by grants from CONICET (Argentina), SeCyT, Universidad Nacional de Córdoba (Argentina), and ICTP Grant No. NET-61 (Italy). Both S.A.P. and S.A.C. are members of CONICET, Argentina.

APPENDIX

When $k_y=0$, Eq. (8) can be written as

$$\hat{J}(k_x,0) = 2\delta(\cos k_x + 1) - S(k_x,0), \tag{A1}$$

with

$$S(k_x,0) \equiv \sum_i \frac{1}{r_{ij}^3}\cos(k_x x_i), \tag{A2}$$

where x_i is the x component of $\vec{r}_i$. This last term can be rewritten as follows:

$$S(k_x,0) = 2\sum_{x=1}^{\infty}\cos(k_x x)R(x) + 2\zeta(3), \tag{A3}$$

with

$$R(x) \equiv \sum_{y=-\infty}^{\infty}\frac{1}{(x^2+y^2)^{3/2}}, \tag{A4}$$

$$\zeta(3) \equiv \sum_{y=1}^{\infty}\frac{1}{y^3} \approx 1.202, \tag{A5}$$

where x,y represents the Cartesian coordinates of each site and $\zeta(x)$ is the Riemann zeta function. $R(x)$ can be approximated by[6]

$$R(x) \approx \int_{-\infty}^{\infty}\frac{dy}{(x^2+y^2)^{3/2}} = \frac{2}{x^2}, \tag{A6}$$

which has an error of 1% in the worst case ($x=1$). Inserting this in Eq. (A3), we get

$$S(k_x,0) \approx 4\sum_{x=1}^{\infty}\frac{\cos(k_x x)}{x^2} + 2\zeta(3) = k_x^2 - 2\pi|k_x| + \frac{2\pi^2}{3} + 2\zeta(3), \tag{A7}$$

which replaced in Eq. (A1) gives expression (12).

*Electronic address: spighin@famaf.unc.edu.ar
†Electronic address: cannas@famaf.unc.edu.ar

[1] R. Allenspach, M. Stampanoni, and A. Bischof, Phys. Rev. Lett. **65**, 3344 (1990).
[2] A. Vaterlaus, C. Stamm, U. Maier, M. G. Pini, P. Politi, and D. Pescia, Phys. Rev. Lett. **84**, 2247 (2000).
[3] K. De'Bell, A. B. MacIsaac, and J. P. Whitehead, Rev. Mod. Phys. **72**, 225 (2000).
[4] P. Politi, Comments Condens. Matter Phys. **18**, 191 (1998).
[5] O. Portmann, A. Vaterlaus, and D. Pescia, Nature (London) **422**, 701 (2003).
[6] R. Czech and J. Villain, J. Phys.: Condens. Matter **1**, 619 (1989).
[7] A. B. MacIsaac, J. P. Whitehead, M. C. Robinson, and K. De'Bell, Phys. Rev. B **51**, 16033 (1995).
[8] I. Booth, A. B. MacIsaac, J. P. Whitehead, and K. De'Bell, Phys. Rev. Lett. **75**, 950 (1995).
[9] A. D. Stoycheva and S. J. Singer, Phys. Rev. Lett. **84**, 4657 (2000).
[10] P. M. Gleiser, F. A. Tamarit, and S. A. Cannas, Physica D **168-169**, 73 (2002).
[11] S. A. Cannas, P. M. Gleiser, and F. A. Tamarit, *Two Dimensional Ising Model with Long-range Competing Interactions*, Recent Research Developments in Physics Vol. 3(II) (Transworld Research Network, India, 2004), pp. 751–780.
[12] S. A. Cannas, D. A. Stariolo, and F. A. Tamarit, Phys. Rev. B **69**, 092409 (2004).
[13] M. Casartelli, L. Dall'Asta, E. Rastelli, and S. Regina, J. Phys. A **37**, 11731 (2004).
[14] S. A. Cannas, M. F. Michelon, D. A. Stariolo, and F. A. Tamarit, Phys. Rev. B **73**, 184425 (2006).
[15] E. Rastelli, S. Regina, and A. Tassi, Phys. Rev. B **73**, 144418 (2006).
[16] O. Portmann, A. Vaterlaus, and D. Pescia, Phys. Rev. Lett. **96**, 047212 (2006).
[17] C. Won, Y. Z. Wu, J. Choi, W. Kim, A. Scholl, A. Doran, T. Owens, J. Wu, X. F. Jin, and Z. Q. Qiu, Phys. Rev. B **71**,

224429 (2005).
[18] Y. Yafet and E. M. Gyorgy, Phys. Rev. B **38**, 9145 (1988).
[19] P. M. Chaikin and T. C. Lubensky, *Principles of Condensed Matter Physics*, 1st ed. (Cambridge University Press, Combridge, 1995).
[20] W. Selke and M. E. Fisher, Phys. Rev. B **20**, 257 (1979).
[21] M. Grousson, G. Tarjus, and P. Viot, Phys. Rev. E **62**, 7781 (2000).
[22] A. B. Kashuba and V. L. Pokrovsky, Phys. Rev. B **48**, 10335 (1993).
[23] A. Abanov, V. Kalatsky, V. L. Pokrovsky, and W. M. Saslow, Phys. Rev. B **51**, 1023 (1995).
[24] S. A. Cannas, M. F. Michelon, D. A. Stariolo, and F. A. Tamarit, arXiv:cond-mat/0701039 (unpublished).